

Ultra-longer fiber cantilever taper for simultaneous measurement of temperature and relative humidity

Min Li(李敏), Jiwen Yin(尹辑文), Weili Yan(闫伟丽), Aimin Cong(丛爱民), Hongjuan Li(李红娟), and Wenqiang Ma(马文强)

Citation: Chin. Phys. B, 2021, 30 (**11**): 114210. DOI: 10.1088/1674-1056/ac012e
Journal homepage: http://cpb.iphy.ac.cn; http://iopscience.iop.org/cpb

What follows is a list of articles you may be interested in

Mid-infrared supercontinuum and optical frequency comb generations in a multimode tellurite photonic crystal fiber

Xu Han(韩旭), Ying Han(韩颖), Chao Mei(梅超), Jing-Zhao Guan(管景昭), Yan Wang(王彦), Lin Gong(龚琳), Jin-Hui Yuan(苑金辉), and Chong-Xiu Yu(余重秀)

Chin. Phys. B, 2021, 30 (**9**): 094207. DOI: 10.1088/1674-1056/abf10f

Distributed analysis of forward stimulated Brillouin scattering for acoustic impedance sensing by extraction of a 2nd-order local spectrum

Yu-Lian Yang(杨玉莲), Jia-Bing Lin(林佳兵), Li-Ming Liu(刘黎明), Xin-Hong Jia(贾新鸿), Wen-Yan Liang(梁文燕), Shi-Rong Xu(许世蓉), and Li Jiang(姜利)

Chin. Phys. B, 2021, 30 (**8**): 084205. DOI: 10.1088/1674-1056/abfcce

Controllable four-wave mixing response in a dual-cavity hybrid optomechanical system

Lei Shang(尚蕾), Bin Chen(陈彬), Li-Li Xing(邢丽丽), Jian-Bin Chen(陈建宾), Hai-Bin Xue(薛海斌), and Kang-Xian Guo(郭康贤)

Chin. Phys. B, 2021, 30 (**5**): 054209. DOI: 10.1088/1674-1056/abd695

Handwritten digit recognition based on ghost imaging with deep learning

Xing He(何行), Sheng-Mei Zhao(赵生妹), and Le Wang(王乐)

Chin. Phys. B, 2021, 30 (**5**): 054201. DOI: 10.1088/1674-1056/abd2a5

Quantum plasmon enhanced nonlinear wave mixing in graphene nanoflakes

Hanying Deng(邓寒英), Changming Huang(黄长明), Yingji He(何影记), and Fangwei Ye(叶芳伟)

Chin. Phys. B, 2021, 30 (**4**): 044213. DOI: 10.1088/1674-1056/abea8d

---

Ultra-longer fiber cantilever taper for simultaneous measurement of temperature and relative humidity*

Min Li(李敏)[1], Jiwen Yin(尹辑文)[1], Weili Yan(闫伟丽)[2], Aimin Cong(丛爱民)[1,†], Hongjuan Li(李红娟)[1], and Wenqiang Ma(马文强)[1]

[1] *Chifeng College, College of Physics and Intelligent Manufacturing Engineering, Chifeng* 024000, *China*
[2] *Inner Mongolia Traffic Vocational and Technical College, Chifeng* 024000, *China*

(Received 16 February 2021; revised manuscript received 12 May 2021; accepted manuscript online 14 May 2021)

An ultra-longer fiber cantilever taper for simultaneous measurement of the temperature and relative humidity (RH) with high sensitivities was proposed. The structure was fabricated by using the simple and cost-effective method only including fiber cleaving, splicing, and tapering. The length of the cantilever taper is about 1.5 mm. The dip A and dip B were measured simultaneously, owing to the ultra-long length and super-fine size, the temperature sensitivities of the dip A and dip B reached as high as 127.3 pm/°C and 0 pm/°C between 25 °C and 50 °C, and the RH sensitivities are −31.2 pm/% RH and −29.2 pm/% RH with a broad RH interval ranging from 20% RH to 70% RH. Besides, the proposed structure showed good linearity in the sensing process and small temperature crosstalk. It will be found in wide applications in environmental monitoring, food processing, and industries.

Keywords: sensor, temperature, humidity

PACS: 42.81.Pa, 92.60.hv, 92.60.jk **DOI:** 10.1088/1674-1056/ac012e

1. Introduction

Optical fiber sensors are widely used in the sensing of pressure, displacement, and temperature because of their small size, light weight, and anti-electromagnetic interference.[1–3] Among them, humidity and temperature are two important factors in various applications such as environmental monitoring, food processing, weather observations, and industries, and often need to be measured simultaneously. Various sensors for measuring relative humidity (RH) and temperature simultaneously have been proposed.[4–8] Among them, the multi-parameter fiber-optic sensors are particularly attractive owing to their outstanding advantages of freedom from electromagnetic interference, wide bandwidth, compactness, possibility of remote sensing,[9–13] as the temperature and RH measurements are often simultaneously performed in diverse, remote, and harsh environments. Recently, fiber-optic sensors for RH and temperature sensing based on different structures have been developed, such as fiber Bragg grating (FBG),[14–18] long-period fiber grating (LPFG),[19] Fabry–Perot interferometer,[20–22] and fiber taper structure.[23,24] The FBG usually was cascaded with a low-finesse Fabry–Perot interferometer.[14–17] These sensors realize the temperature and RH simultaneous sensing by analyzing the interference peaks shift and the peaks loss variations. Although they have good sensitivities, the detection accuracy of peaks loss is seriously affected by system power fluctuations, which cause the detection error. To improve the detection accuracy, fiber-optic sensors depended on the wavelengths shift and the sensitivity matrix method has been proposed to achieve dual-parameter measurement of RH and temperatures. The sensing head is based on an LPFG coated with silica nanospheres in-line with an FBG,[16] and fiber-coated polyvinyl alcohol (PVA) film for RH sensing, and FBG for temperature measurements.[25,26] Both temperature and RH are spectrally resolved. However, the organic active film coated on fiber limits RH and environmental/chemical stability of sensors, and the preparation processes of sensors are complex.

In this paper, an ultra-longer fiber cantilever taper for measuring RH and temperature simultaneously with high sensitivities was proposed. The simple splicing technique was used to fabricate the structure by using a fiber splicer (KL-300T). The length of the ultra-longer fiber cantilever taper about 1.5 mm. The interference spectrum exhibits several peaks with distinct sensitivities with respect to the changes in both RH and temperatures. The two peaks were chosen to measure RH and temperature sensitivities, and the RH sensitivities are −31.2 pm/% RH and −29.2 pm/% RH. The temperature sensitivities are 127.3 pm/°C and 0 pm/°C. By using the sensitivity matrix method, the RH and temperature can be simultaneously determined. Therefore, the proposed sensor has great applications in chemical, biomedical, and environ-

*Project supported by the Scientific Research Project of Institutions of Higher Learning in Inner Mongolia Autonomous Region, China (Grant No. NJZY19214), the Natural Science Foundation of Inner Mongolia Autonomous Region, China (Grant No. 2018MS05064), the Education and Teaching Research Project of Chifeng College (Grant No. JYXMY202025), the Applied Model Curriculum Construction Project of Chifeng College (Grant No. SFK20200904), and the Construction Project of the Key Laboratory of Chifeng College (Grant No. CFXYZD202007).

†Corresponding author. E-mail: c15026710904@163.com

© 2021 Chinese Physical Society and IOP Publishing Ltd

mental industry due to its no crosstalk, good chemical stability, and simple fabrication process.

2. Fabrication and theory

The fiber cantilever taper was fabricated by using two-step arc discharge fiber tapering method.[27] The fabrication process diagram is shown in Fig. 1. Firstly, the end-faces of the two single mode fibers (SMFs) were cut flat and fixed on the fiber fixtures controlled by two stepping motors respectively, as shown in Fig. 1(a). Secondly, the two SMFs were heated by using arc discharge. Meanwhile, the two sides of the SMFs were pulled at constant speed. The fiber tapers with regular shape and smooth surface can be achieved, which is shown in Fig. 1(b). Thirdly, one side of the structure in the second step was fixed, and another side continued to be pulled. To make sure that the fiber cantilever taper has sufficient length and uniformed shape, a faster and constant pulling speed was used. Finally, an ultra-longer fiber cantilever tapering was obtained. The schematic diagram and the optical image of the fiber cantilever taper was shown in Figs. 1(c) and 1(d). Form Fig. 1(d) it can be seen that, the length of the taper is about 1.5 mm, and there is a regular shape. Both the length and the shape of the fiber cantilever taper depend on the pulling speed in the two-step arc discharge fiber tapering processes. It is worth mentioning that, with the increasing of the cantilever taper length, the waist size of the taper got thinner and thinner.

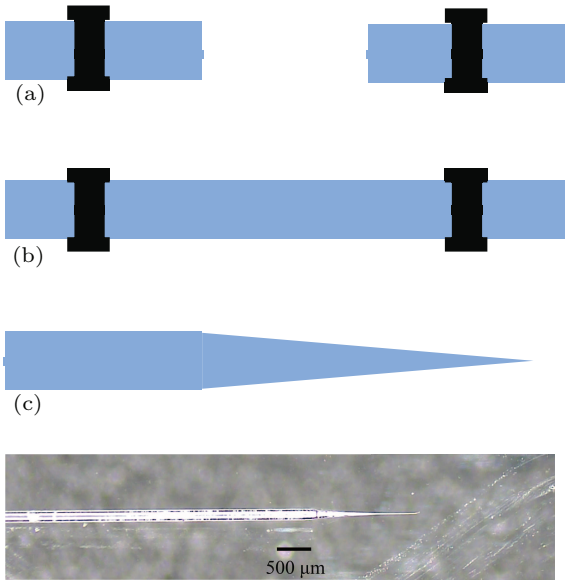


Fig. 1. (a)–(c) The fabrication diagram of the fiber cantilever taper by using arc discharge fiber tapering method. (d) The picture of fabricated fiber cantilever taper.

The reflection spectrum of the proposed structure was measured by using an optical spectrum analyzer (OSA, AQ6370D) and broad-band source (BBS, YSL SC-5) through a circulator. The spectrum was shown in Fig. 2. As the fiber cantilever taper was structured with regular shape and smooth surface, it shows obvious inference peaks in the reflection spectrum, and the maximum of the contrast achieved 22 dB.

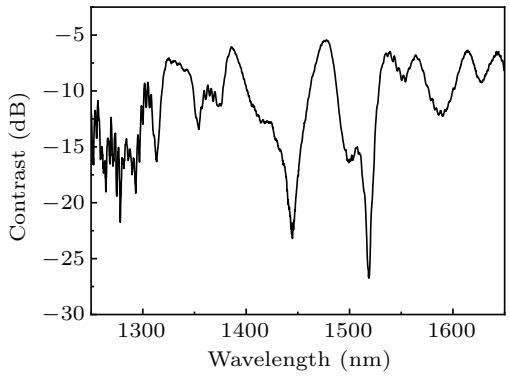


Fig. 2. Reflection spectrum of fiber cantilever taper.

The reflection spectrum is obtained by interference of core mode and cladding mode, and the phase can be given as[28]

$$\Phi = \frac{4\pi\Delta n_{\text{eff}} L}{\lambda}, \tag{1}$$

where Δn_{eff} is the effective refractive index difference between the core and cladding modes. λ is the input light wavelength, and L is the effective length of fiber taper. The central wavelength of the peaks is given as follows:

$$\lambda_m = \frac{4\Delta n_{\text{eff}} L}{(2m+1)}, \tag{2}$$

where m is the interference order. When the relative humidity increases, the refractive index of the environment surrounding fiber taper increase by δn_{eff}. Since the refractive index of the core mode stays almost constant, the effective refractive index decreases by δn_{eff}. Therefore, the central wavelength of the interference peak has shift to a shorter wavelength

$$\delta\lambda_m = 4\pi\delta n_{\text{eff}} L. \tag{3}$$

As the environment temperature changes, the central wavelengths of the interference fringes are determined by the difference of effective refractive index and the length of taper, which can be given as

$$\delta\lambda_m = 4\pi(\delta n_{\text{eff}} L + \Delta n_{\text{eff}}\delta L). \tag{4}$$

The resulting interference fringes formed in the wavelength domain exhibit two distinct groups of sensitivities with the variations of RH and temperatures. Consequently, by using the sensitivity matrix method, the RH and ambient temperature can be simultaneously determined.

3. Experiment results and discussion

To investigate the response of the ultra-longer fiber cantilever taper to RH, the fiber cantilever taper was connected to BBS and OSA through a circulator as shown in Fig. 3. Meanwhile, the fiber cantilever taper was put into the sealed temperature and humidity controllable chamber (Kingjo, CK-80G) where the RH is controlled and monitored through LED

screens. Theoretically, the humidity sensor can be controlled from 20% RH to 98% RH. In this experiment, the RH was set from 20% RH to 70% RH with a step of 10% RH, and the temperature was fixed at 20 °C in the process of humidity measurements.

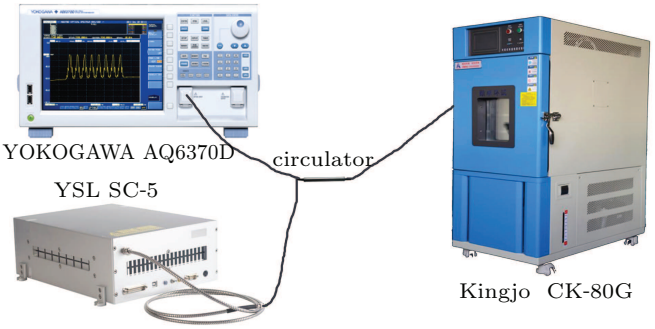


Fig. 3. Diagram of temperature and relatively humidity test device.

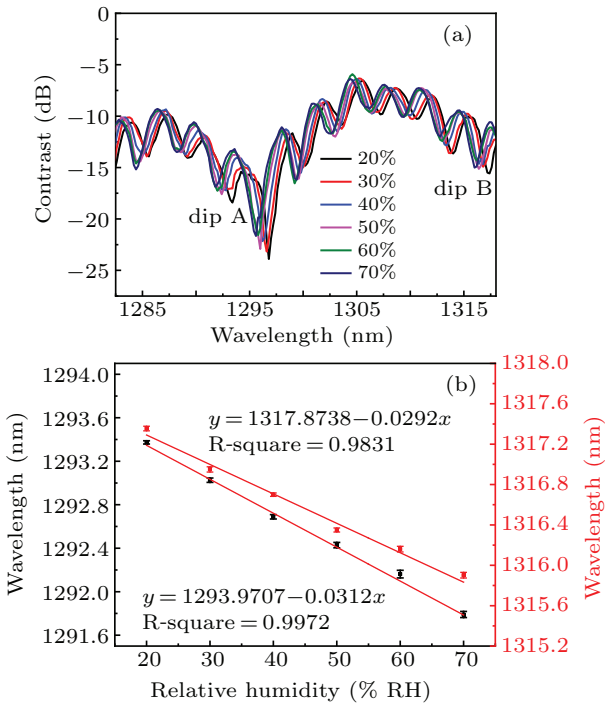


Fig. 4. (a) Measured interference spectrum changing with the RH varying, (b) responding of dips A and B to the different RH.

The dips A and B were chosen to measure the interference spectrum shifts in detail with the variations of RH and temperatures. With the RH increasing from 20% RH to 70% RH at constant temperature, the dips A and B shifted to the shorter wavelength, which is shown in Fig. 4(a). From Fig. 4(a), with the RH varying from 20% RH to 70% RH, the wavelengths of the dip A and dip B changed from 1293.356 nm to 1291.768 nm and 1317.360 nm to 1315.902 nm, respectively. Three repeated experiments were done. We calculated the mean central wavelength and standard deviation of two dips at each RH recording point, and the standard deviation was shown in the form of error bars, as shown in Fig. 4(b). The mean central wavelengths of the dip A at each RH are 1293.373 nm, 1293.026 nm, 1292.689 nm, 1292.429 nm, 1292.162 nm, and 1291.790 nm. The mean central wavelengths of the dip B at each RH are 1317.355 nm, 1316.953 nm, 1316.706 nm, 1316.354 nm, 1316.169 nm, and 1315.925 nm. Linear fitting results of these points as shown in Fig. 4(b). From Fig. 4(b) the RH sensitivities of dips A and B are −31.2 pm/% RH and −29.2 pm/% RH, respectively. That is because that the effective refractive index difference between the core and cladding modes decreases with the temperature increasing. From Fig. 4(b), we can see that the fiber cantilever taper for the RH sensing has excellent linear relationship and good repeatability, and the R-square of dip A and dip B are 0.997 and 0.983.

To investigate the response of the fiber cantilever taper to temperature, the temperature of the temperature and humidity controllable chamber was changed from 25 °C to 50 °C at a step of 5 °C, and the RH was fixed at 20% RH in the process of temperature measurements. The length and the refractive index change with temperature elevation for the thermal expansion effect and thermo-optic effect. As a result, the wavelength of the dips A and B shifted to long wavelength with temperature increasing, as is shown in Fig. 5(a). From Fig. 5(a), with the temperature increasing, the central wavelengths of the dip A and dip B shift from 1293.160 nm to 1296.420 nm and 1313.550 nm to 1313.900 nm, respectively. Three repeated experiments were done. The mean wavelength shifts and error bars of measurements at each temperature point were calculated, which were shown in Fig. 5(b). The mean central wavelength details of dip A are 1293.169 nm, 1294.020 nm, 1294.451 nm, 1295.048 nm, 1295.822 nm, and 1296.446 nm at 25 °C, 30 °C, 35 °C, 40 °C, 45 °C, and 50 °C, respectively. The details of the dip B are 1313.552 nm, 1313.653 nm, 1313.907 nm, 1313.704 nm, 1313.651 nm, and 1313.983 nm at each temperature recording point. Linear fitting of the data in Fig. 5(b) is performed, and the linear fitting results show that the sensor tip for sensing the temperature is with excellent linear relationship and good repeatability, and the temperature sensitivities of dips A and B are 127.3 pm/°C and 0 pm/°C, respectively. Because the thermal optical coefficient of the fiber is positive and is much larger than that of air, δn_{eff} increases with temperature rise. At the same time, the length of fiber taper is changed with the temperature varying due to the thermal expansion effect. According Eq. (4), the varying of interference fringes with temperature depend on the length and effective refractive index. In addition, from Fig. 5(b), the R-square of the dip A is 0.993 at the temperature measurement range of 25 °C–50 °C.

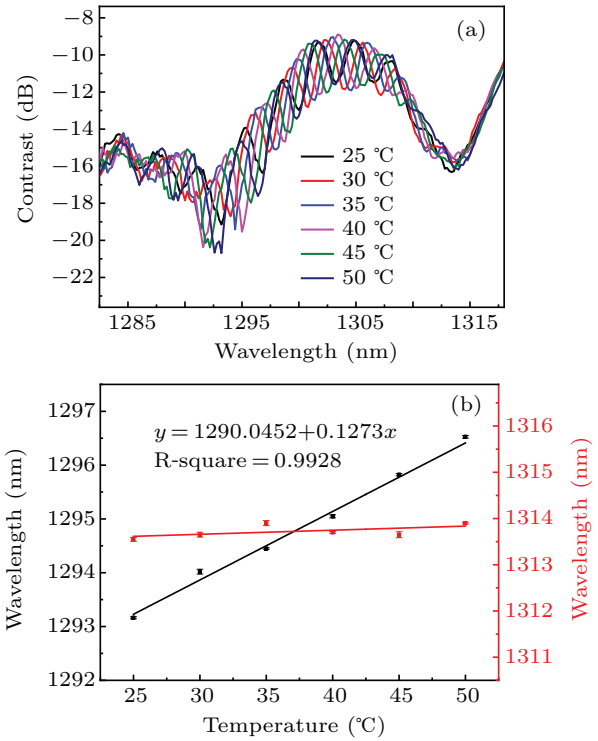


Fig. 5. (a) Measured interference spectrum changing with the liquid temperature varying, (b) responding of dips A and B to different temperatures.

The experimental results show the sensitivities of the two dips to RH and temperature respectively. The sensitivities of dip A and dip B to RH are −31.2 pm/% RH and −29.2 pm/% RH, respectively. The sensitivities of dip A and dip B to temperature are 127.3 pm/°C and 0 pm/°C, respectively. These sensitivities are used to calculate the dual parameter matrix in Eq. (1)

$$\begin{bmatrix} \Delta\lambda_{\text{dip A}} \\ \Delta\lambda_{\text{dip B}} \end{bmatrix} = \begin{bmatrix} S_{\text{RHA}} & S_{\text{TA}} \\ S_{\text{RHB}} & S_{\text{TB}} \end{bmatrix} \begin{bmatrix} \Delta RH \\ \Delta T \end{bmatrix}, \tag{5}$$

where $\Delta\lambda_{\text{dip A}}$ and $\Delta\lambda_{\text{dip B}}$ are the wavelength shifts of dips A and dip B, respectively. ΔRH and ΔT are the RH and temperature changes. S_{RHA}, S_{TA}, S_{RHB}, S_{TB} are the matrix coefficients for experimental results showing that $S_{\text{RHA}} = -31.2$ pm/% RH, $S_{\text{TA}} = 127.3$ pm/°C, $S_{\text{RHB}} = -29.2$ pm/% RH, and $S_{\text{TB}} = 0$ pm/°C.

The sensitivities of the RH and temperature at any point can be easily determined by solving Eq. (5). The follwoing equation shows the solved inverse matrix to obtain the applied RH and temperature at any given spectral shift:

$$\begin{bmatrix} \Delta RH \\ \Delta T \end{bmatrix} = \begin{bmatrix} S_{\text{RHA}} & S_{\text{TA}} \\ S_{\text{RHB}} & S_{\text{TB}} \end{bmatrix}^{-1} \begin{bmatrix} \Delta\lambda_{\text{dip A}} \\ \Delta\lambda_{\text{dip B}} \end{bmatrix}. \tag{6}$$

4. Conclusion

In summary, a fiber cantilever taper with high RH and temperature sensitivities has been proposed and fabricated for simultaneous measuring of the temperature and RH by using the simple fabrication process. The dips A and B in the interference spectrum were chosen to measure the RH and temperature. The RH of the dips A and B are −31.2 pm/% RH and −29.2 pm/% RH, and the temperature sensitivities are 127.3 pm/°C and 0 pm/°C. Simultaneous measurement of the RH and temperature can be achieved by using the sensitivity matrix method. Thus, it has great application in environmental monitoring, food processing, and industries.

References

[1] Zhang Y S, Qiao X G and Shao M 2015 *Chin. Phys. Lett.* **32** 64208
[2] Liu N L, Liu S H and Lu P X 2014 *Chin. Phys. Lett.* **31** 94204
[3] Wen X D, Ning T G and You H D 2014 *Chin. Phys. Lett.* **31** 034203
[4] Ren S, Shang K, Cui M, Wang L, Pu J and Yi P 2019 *J. Mater. Sci.* **54** 11889
[5] Zhao Y, Peng Y, Chen M Q and Tong R J 2018 *Sens. Actuators B: Chem.* **263** 312
[6] Zhang C, Zhang W, Webb D and Peng G 2010 *Electron. Lett.* **46** 643
[7] Rajan D, Verho J, Kreutzer J, Välimäki H, Ihalainen H and Lekkala J 2017 *IEEE International Symposium on Medical Measurements and Applications* 470
[8] Tadele S and Emana G 2017 *J. Hortic. For.* **9** 66
[9] Berruti G, Consales M, Giordano M, Sansone L, Petagna P and Buontempo S 2013 *Sens. Actuators B: Chem.* **177** 94
[10] Shin J, Yoon M and Han Y 2016 *J. Lightwave Technol.* **34** 4511
[11] Wu Y, Zhang T, Rao Y and Gong Y 2011 *Sens. Actuators B: Chem.* **155** 258
[12] Fu H, Jiang Y, Ding J and Zhang J 2017 *IEEE Sens. J.* **17** 644
[13] Sun L, Semenova Y, Wu Q, Liu D, Yuan J and Sang X 2016 *IEEE Photon. J.* **8** 1
[14] Mathew J, Semenova Y and Farrell G 2013 *IEEE Sens. J.* **13** 1632
[15] Arregui F G, Matías I R, Cooper K L and Claus R O 2002 *IEEE Sens. J.* 482
[16] Shao M, Zang Y, Qiao X, Fu H and Jia Z 2017 *IEEE Sens. J.* **17** 1302
[17] Woyessa G, Pedersen J K M, Fasano A, Nielsen K, Markos C, Rasmussen H K and Bang O 2017 *Opt. Lett.* **42** 1161
[18] Zhang S, Dong X, Li T, Chan C and Shum P 2013 *Opt. Commun.* **303** 42
[19] Viegas D, Hernaez M, Goicoechea J, Santos J L, Araújo F M, Arregui F and Matias I R 2011 *IEEE Sens. J.* **11** 162
[20] Yang M, Xie W, Dai Y, Lee D, Dai J, Zhang Y and Zhuang Z 2014 *Opt. Express* **22** 11892
[21] Pevec S and Donlagic D 2015 *Opt. Lett.* **40** 5646
[22] Yulianti I, Supa'at A S M, Idrus S M and Anwar M R S 2013 *Optik* **124** 3919
[23] Zhong Y, Tong Z, Zhao X, Zhang W, Qin J, Gao W, Chen X 2019 18*th International Conference on Optical Communications and Networks*
[24] Zhong Y, Tong Z, Zhang W, Qin J and Gao W 2019 *Appl. Opt.* **58** 7981
[25] Zhang S, Dong X, Li T, Chan C C and Shum P P 2013 *Opt. Commun.* **303** 42
[26] Cheng Q H, Zhang A L, Pan H G, Li W and Sun C 2020 *Optoelectron. Lett.* **16** 0428
[27] Liu Y, Lang C, Wei X and Qu S L 2017 *Opt. Express* **25** 7797
[28] Tian Z, Yam S S H and Loock H P 2008 *Opt. Lett.* **33** 1105